Temperature dependence of elastocaloric effect in a microstructurally graded NiTi alloy

Junyu Chen [a,b], Wenqiang Wang [a], Qi Zhang [a], Liping Lei [a], Upadrasta Ramamurty [b,c,1], Gang Fang [a,*]

[a] *State Key Laboratory of Clean and Efficient Turbomachinery Power Equipment, Department of Mechanical Engineering, Tsinghua University, Beijing 100084, China*

[b] *School of Mechanical and Aerospace Engineering, Nanyang Technological University, Singapore 639798, Republic of Singapore*

[c] *Institute of Materials Research and Engineering (IMRE), Agency for Science, Technology and Research (A*STAR), Singapore 138634, Republic of Singapore*

Abstract

The temperature dependence of elastocaloric cooling properties of a NiTi alloy with a grain size gradient, which was obtained by cold rolling and subsequent laser surface annealing, was evaluated and compared with those of coarse-grained and as-rolled NiTi. Results show that the adiabatic temperature change ($|\Delta T_{ad}|$) and cooling efficiency of the gradient-structured NiTi are significantly enhanced over a wider temperature span (T_{span}), making it a superior elastocaloric refrigerant candidate. Detailed analyses show that while the fine grains present in the core reduce the global martensitic autocatalytic nucleation potency and increase strength to broaden T_{span}, the coarser grains near the surfaces accommodate interlayer deformation to improve $|\Delta T_{ad}|$. The work provides a method for overcoming the trade-off between cooling capacity and service temperature span of elastocaloric materials.

* Corresponding author; e-mail address: fangg@tsinghua.edu.cn (G. Fang).

[1] Upadrasta Ramamurty was an Editor of the journal during the review period of the article. To avoid a conflict of interest, Upadrasta Ramamurty was blinded to the record and another editor processed this manuscript.

Keywords: Shape memory alloys (SMA); Functionally graded materials (FGM); Elastocaloric cooling; Laser annealing; Martensitic phase transformation

Superelastic NiTi is a leading candidate for solid-state refrigerant applications, wherein the elastocaloric cooling, associated with the latent heat of stress-induced martensitic transformation (MT), is exploited [1-3]. In a number of potential application scenarios (such as deep sea or outer space applications) [4], it becomes mandatory for the NiTi refrigerant to continue showing large adiabatic temperature changes ($|\Delta T_{ad}|$) over a broad temperature span (T_{span}). However, the currently-available NiTi, with the typical first-order MT, exhibits, in general, an acceptable $|\Delta T_{ad}|$ only within a narrow T_{span} (tens of Kelvin) [5, 6], which limits the incorporation of NiTi into wider industrial applications.

Several efforts have been made to expand T_{span} of NiTi-based caloric materials by tailoring the sharp MT toward a diffuse one through composition or microstructural engineering. However, this is often accomplished at the expense of $|\Delta T_{ad}|$ [5, 7-11], as there is a trade-off between T_{span} and $|\Delta T_{ad}|$ [1, 5, 12]. Thus, simultaneously achieving large $|\Delta T_{ad}|$ and wide T_{span} in NiTi remains a challenge. Recent research has shown that grain size affects both T_{span} and $|\Delta T_{ad}|$ significantly [5, 6, 12, 13]; while $|\Delta T_{ad}|$ increases with the grain size, T_{span} decreases. Specifically, large $|\Delta T_{ad}|$ and wide T_{span} are often observed only in the freestanding coarse- and fine-grained NiTi, respectively. On this basis, it is reasonable to conjecture that structural components with graded grain sizes could offer both wide T_{span} and large $|\Delta T_{ad}|$ in NiTi [14, 15].

In our recent work [14, 16, 17], we fabricated a gradient-structured (GS) NiTi with a nanocrystalline core sandwiched between two coarse-grained laminates. This was accomplished by laser surface annealing on the NiTi strips that were severely-deformed *a priori*. We demonstrated, via experiments and simulations, that the gradient structure is beneficial to increase the cooling potential of NiTi at room temperature. In the current study, the elastocaloric cooling performance of GS NiTi is evaluated over the temperature range of -60 to 140 ℃ and compared to those of as-rolled (AR) and coarse-grained (CG) NiTi.

The processing steps involved in fabricating GS NiTi are detailed in [14]. They are summarized here. The as-received 1.5-mm-thick $Ni_{50.8}Ti_{49.2}$ (at.%) sheets were first homogenized at 800 ℃ for 1 h and then were repeatedly cold rolled to achieve a final thickness of ~ 1.0 mm (1/3 thickness reduction). After polishing the as-rolled sheets, laser surface annealing was performed (using a Renishaw AM250 device) on their upper and lower surfaces to introduce gradient microstructures. A laser power of 100 W, scanning speed of 1000 mm s^{-1}, and hatch spacing of 30 μm were used. For comparison, the properties of AR NiTi and its uniformly annealed (at 500 ℃ for 380 s) counterpart with coarse grains were also studied. Transmission electron microscope (TEM, JEM-2100F) and *in-situ* cooling X-ray diffraction (XRD) using a Rigaku Smartlab 9 kW diffractometer were employed to characterize microstructures. The TEM foils were prepared by twin-jet electro-polishing, and the X-rays were projected onto the upper surface of the sheets. Tensile specimens with a gauge section of ~ 20 × 3 × 1 mm^3 in dimension were cut from the prepared sheets along the rolling direction

and then were tested using a universal testing machine (Shimazu, AG-X) equipped with a thermostatic chamber. The temperature changes were monitored by using the T-type thermocouple wires welded on the surface of specimens under a recording frequency of 100 Hz, and elastocaloric cooling performances were investigated at different ambient temperatures from -60 to 140 ℃.

Microstructural details of AR, CG, and GS NiTi are already presented in [12, 14]. For completeness, they are summarized here. The bright-field TEM micrograph (Fig. 1a) and the selected-area electron diffraction (SAED) pattern suggest that AR NiTi is composed of nanosized crystals (i.e., austenite B2 and martensite B19′ with a mean grain size of ~ 12 nm) embedded within an amorphous phase, resulting from severe plastic deformation [14, 18]. High-resolution TEM (Fig. 1b) and the corresponding fast Fourier transform images (the three insets in Fig. 1b) further confirm the coexistence of these phases. After uniform annealing, devitrification, recovery and recrystallization occur in the AR matrix, resulting in a relatively coarse-grained (CG) austenitic structure with an average diameter of 75 nm (Figs. 1c and d). Representative microstructures at various depths of GS NiTi, with the corresponding SAED patterns, are shown in Fig. 1e. The average grain sizes decrease markedly from ~ 110 nm at the near topmost surface to ~ 12 nm at the 300-μm-deep layer. These microstructural changes are accompanied by the SAED patterns becoming gradually continuous [14].

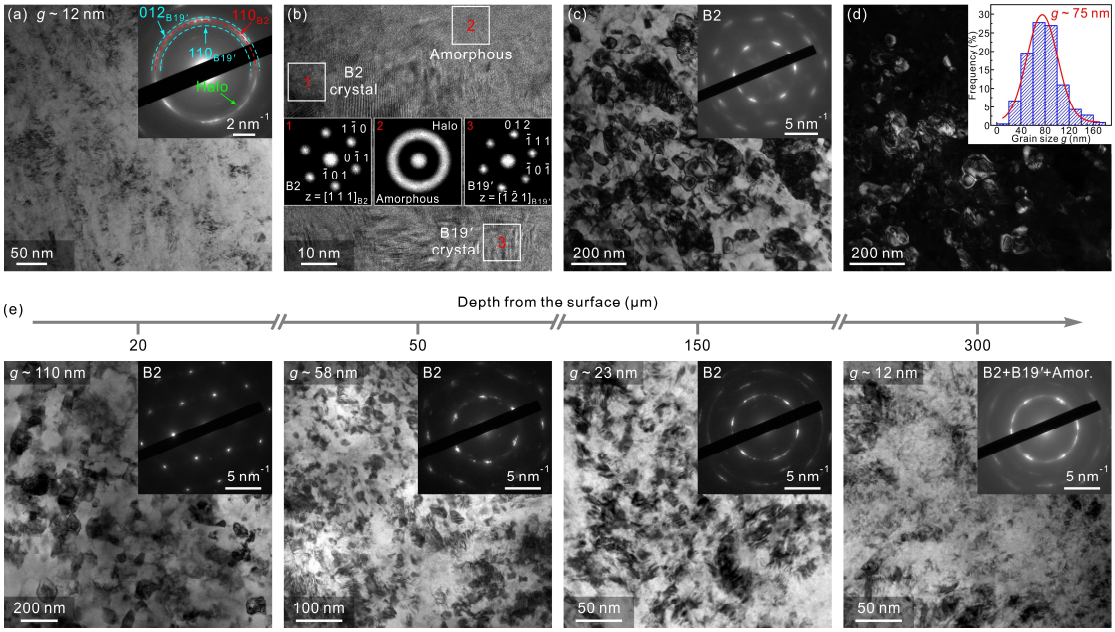

Fig. 1. Results of microstructural characterization for (a) - (b) as-rolled (AR), (c) - (d) coarse-grained (CG) and (e) gradient-structured (GS) NiTi observed at room temperature (~ 25 °C).

The room temperature tensile stress-strain response of GS NiTi is compared with those of AR and CG NiTi in Fig. 2a. While GS NiTi exhibits a moderately hardening-type phase transformation behavior, AR and CG NiTi exhibit quasi-linear (indicating its brittleness) and the plateau-type superelastic responses, respectively. Figure 2b shows the representative full-field strain patterns of longitudinal deformation within them during loading and unloading. While the CG NiTi exhibits localized MT with Lüders bands, both AR and GS NiTi exhibit a rather uniform deformation [19, 20]. The findings confirm that the fine and coarse grains in GS NiTi act synergistically, resulting in the observed characteristics of MT.

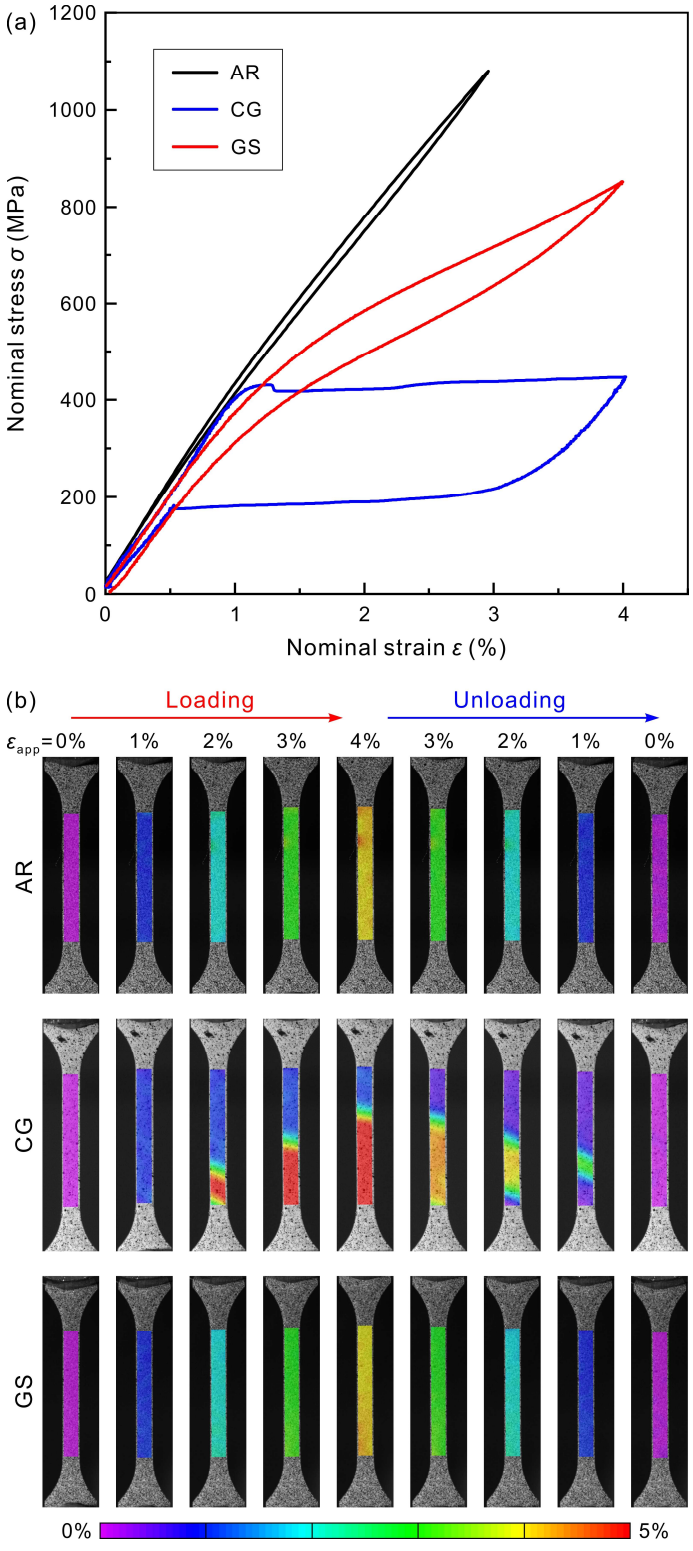

Fig. 2. (a) Isothermal stress-strain curves and (b) representative full-field longitudinal strain patterns of as-rolled (AR), coarse-grained (CG) and gradient-structured (GS) NiTi at room temperature (~ 25 °C).

Next, we study the temperature dependence of elastocaloric properties of AR, CG and GS NiTi upon isothermal loading (1×10^{-4} s^{-1}) to a pre-designated strain (ε_{max} =

3.5% for both CG and GS NiTi) and then rapid unloading (5×10^{-2} s^{-1}) to approach the adiabatic condition in an approximate manner. Since AR NiTi is not ductile, a ε_{max} = 2.5% was used to prevent any possible damage; full recovery was observed over the entire measured temperature range owing to its thermodynamic stability [5, 21] (Fig. 3a). By contrast, the superelasticity of CG NiTi is restricted within a narrow T_{span} ($40 < T < 80$ °C); in it nonrecoverability increases with decreasing T due to the instability of the B2 phase at lower T while plastic deformation from dislocation slip emerges at T = 100 °C and failure soon ensues (T = 120 °C) upon further heating. In contrast, GS NiTi inherits the high thermodynamic stability from its fine-grained microstructural constituents and thus exhibits a good superelasticity over a wide T_{span} from -20 to 100 °C.

The variations in the forward transformation stress (σ_{tr}) of AR, CG and GS NiTi are plotted as a function T in Fig. 3b. All the σ_{tr}-T curves follow the Clausius-Clapeyron relationship. The estimated $d\sigma_{tr}/dT$ of 1.15 MPa/°C in AR NiTi suggests a sluggish MT in it. In comparison, GS NiTi has a relatively mild MT ($d\sigma_{tr}/dT$ = 5.02 MPa/°C), which is marginally smaller than that noted for CG NiTi ($d\sigma_{tr}/dT$ = 6.51 MPa/°C). The temperature dependence of the degree of superelasticity in the three microstructures is illustrated through Figs. 3c and d. It is found that GS NiTi maintains small residual strain (ε_r) and low stress hysteresis (σ_{hy}) over a wider T in contrast to CG NiTi that exhibits poor recoverability and structural stability. While negligible ε_r and small σ_{hy} are observed in AR NiTi, its limited ductility and the resultant weak caloric effect (Supplementary Fig. S1) would be detrimental in practical applications.

The superelastic temperature window of NiTi is mainly governed by both the critical stress for the initiation of dislocation slip (upper bound) and the thermal stability of the B2 phase (lower bound) [22, 23]. In general, a higher yield strength (σ_y) and a lower thermal sensitivity of MT ($d\sigma_{tr}/dT$) contribute to a wider superelastic window [23, 24]. The increased σ_y due to the Hall-Petch effect [25] and the reduced $d\sigma_{tr}/dT$ (i.e., the elevated MT barrier) caused by grain refinement [26, 27] are responsible for the broader superelastic T_{span} in AR NiTi relative to that of CG NiTi (Figs. 3a and b). For GS NiTi, the abundance of grain boundaries (GBs) in the fine-grained core, inherited from the severe cold rolling, inhibits the thermally induced MT due to the significantly increased transformation energy barrier [27, 28]. Simultaneously, GBs improve σ_y through the grain boundary strengthening mechanism [25, 29, 30]. As a result, greater global undercooling (lower bound) is required for martensitic autocatalytic nucleation in coarse-grained regions of GS NiTi for satisfying deformation accommodation of neighboring heterogeneous regions. Dislocation plasticity is prevented even at high temperatures (upper bound), thereby expanding superelastic T_{span} of GS NiTi. Since the superelasticity and the elastocaloric effect share the same physical basis (i.e., stress-induced MT) [1, 31], a large $|\Delta T_{ad}|$ is retained over a wide T_{span} in GS NiTi.

In GS NiTi, ΔT_{ad} varies from -4.55 to -9.78 °C, over a T of -40 and 140 °C, for an ε_{max} of 3.5% (Fig. 3e). It is found that the absolute value of ΔT_{ad} first increases and then decreases as T rises, because the residual deformation is reduced whereas the critical MT stress is elevated with increasing T (Fig. 3a). To evaluate the refrigeration potential of GS NiTi, we compare its cooling performance with that of AR and CG NiTi, as

shown in Figs. 3f - h. As the combined consequence of transformation hysteresis and plastic work [6, 32, 33], the energy dissipation ΔW (i.e., the hysteresis loop area as defined in Fig. 3a) of the alloy in all the three microstructural conditions shows strong temperature dependence. Notably, ΔW of GS NiTi is always far lower than that of CG NiTi over the entire T window examined, and a 65% reduction in ΔW is observed at T = 0 °C. A homogeneous and stabilized MT (Fig. 2b) coupled with an improved matrix strength (Fig. 3a) contribute to the lower ΔW in GS NiTi relative to CG NiTi [12, 33, 34]. An extremely low ΔW of AR NiTi is due to the small deformation (ε_{max} = 2.5%) and the near-linear mechanical response (Fig. 3a).

To directly measure the refrigeration capacity of NiTi in the three microstructural states, $|\Delta T_{ad}|$ (caused by latent heat absorption) is plotted as a function of T in Fig. 3g. $|\Delta T_{ad}|$ of CG NiTi precipitously reduces with decreasing T, due to thermodynamic instability of B2. It also suffers from high-temperature plasticity and failure. These features are typical of the elastocaloric effect occurring over a narrow T_{span} of NiTi with characteristic first-order MT. A broadened T_{span} coupled with diminished ΔW in AR NiTi results in a poor $|\Delta T_{ad}|$ (Fig. 3g). These findings further confirm the trade-off between T_{span} and $|\Delta T_{ad}|$ in conventional NiTi. In GS NiTi, however, these two conflicting cooling metrics are reconciled: $|\Delta T_{ad}|$ is improved by as much as 160% while T_{span} is twice that of CG NiTi. The large $|\Delta T_{ad}|$ of GS NiTi is mainly attributed to the gradient structure effect [14, 16, 17], where the mechanical incompatibility and the resultant deformation accommodation among heterogeneous domains enable a strong caloric effect. The material's coefficient of performance (COP_{mat}), computed

from the ratio of $\left|C_p\Delta T_{ad}\right|$ (C_p: specific heat capacity) to ΔW [15], is a parameter that can be used to evaluate its cooling efficiency. As seen from Fig. 3h, the GS NiTi exhibits a multifold increase (up to 588%) in COP_{mat} over a wide T_{span}, as compared to CG NiTi. Besides, the functional fatigue performance of GS NiTi is also far superior to that of CG NiTi (Fig. S2).

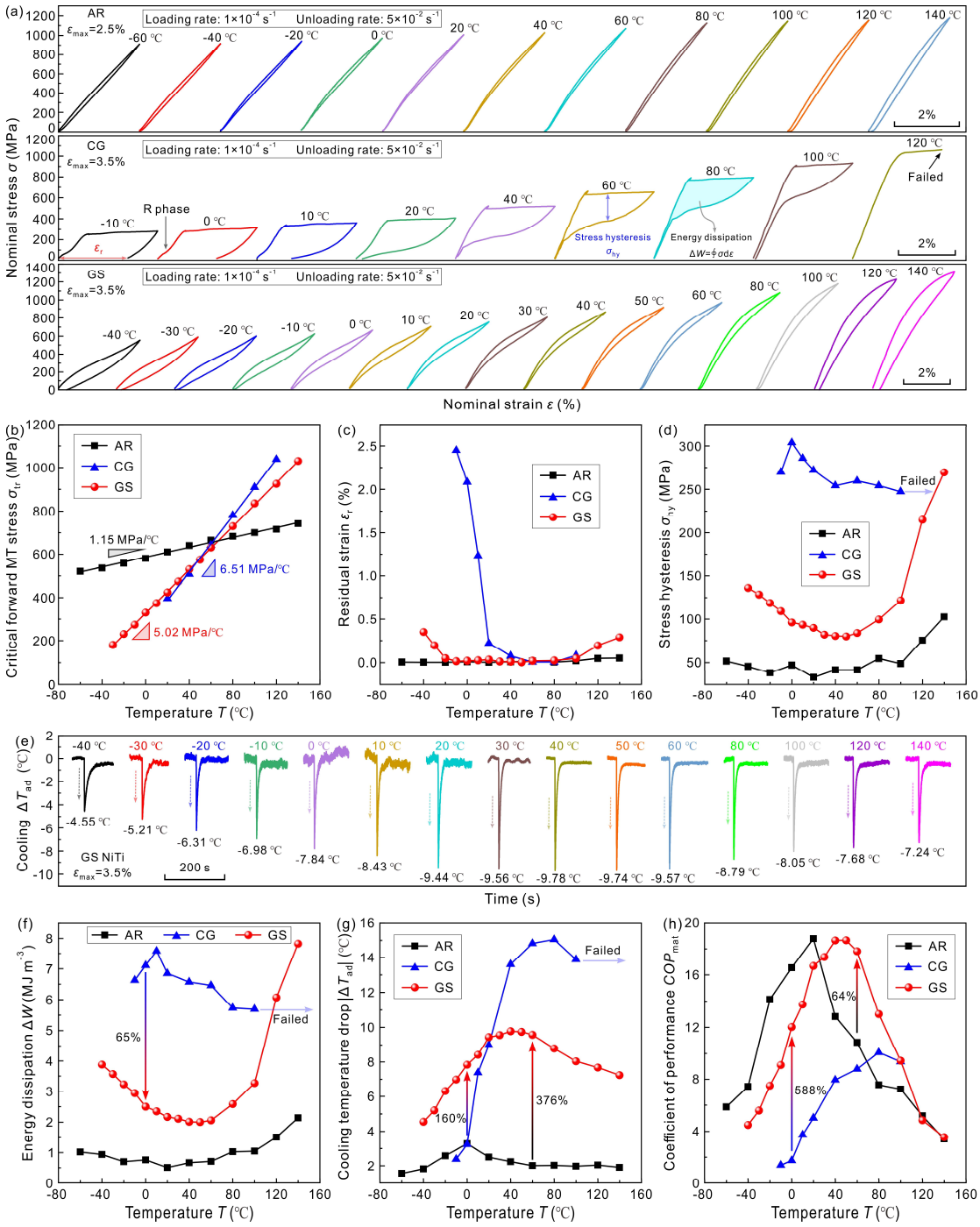

Fig. 3. A comparison of temperature-dependent elastocaloric cooling performances among AR, CG and GS NiTi. (a) Stress-strain curves upon isothermal loading and adiabatic unloading, and the corresponding (b) critical forward transformation stress, (c) residual strain and (d) stress hysteresis. (e) Evolution of the average temperature change of the GS NiTi over a wide temperature range. Variations of (f) energy dissipation, (g) cooling temperature drop and (h) coefficient of performance with testing temperatures.

The physical origin of the above temperature-dependent elastocaloric properties is further elucidated by examining the thermally induced structural change through XRD performed at different *T*. The XRD spectra obtained from -60 to 100 °C are shown in Fig. 4. For AR NiTi, the intensities of the diffraction peaks belonging to the B2 and B19′ phases remain nearly-invariant in the cooling process, which confirms the suppression of thermally induced MT. It also accounts for the thermodynamic stability of elastocaloric effect in it (Fig. 3g). On the contrary, the $(110)_{B2}$ diffraction peak of CG NiTi gradually splits into $(11\bar{2})_R$ and $(300)_R$ peaks of the R phase with cooling. Besides the emergence of $(103)_{B19'}$, the existence of the R phase generated by the assistance of dislocations, rather than precipitates (Fig. 1c and d) [35-37], is also confirmed in the stress-strain curves with a 'knee point' ($\sigma \sim 60$ MPa) observed during loading (Fig. 3a). It should be noted that the observed R phase is a cooling-induced intermediate phase between austenite and martensite, and does not exist in the initial material around room temperature (Fig. S3). The high temperature sensitivity of the crystal structure of CG NiTi, which degrades the reverse MT and thus latent heat absorption, provides a direct rationale for $|\Delta T_{ad}|$ being limited to a narrow T_{span} in it. By comparison, only the diffraction peaks of B2 are detected in GS NiTi over the entire testing temperature range. Such high stability, which stems from the unique gradient structure, makes GS NiTi a superior refrigerant candidate (Fig. 5).

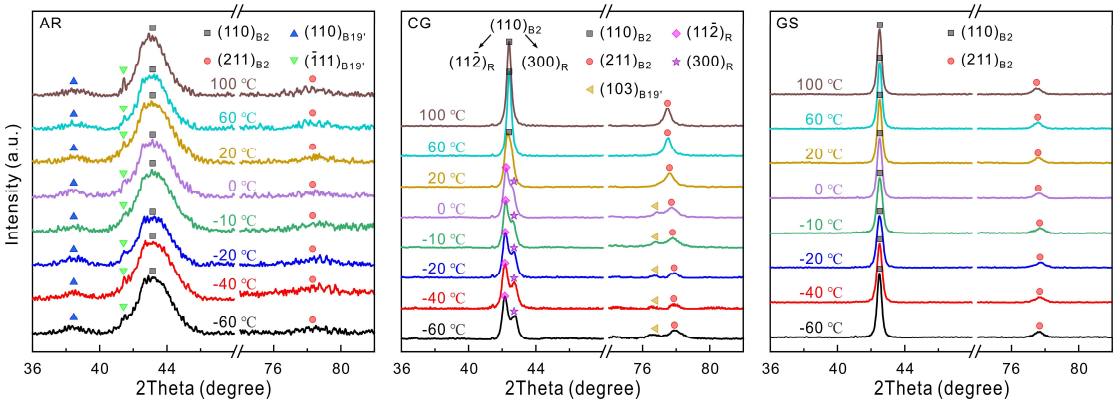

Fig. 4. Temperature dependence of XRD spectra of AR, CG and GS NiTi.

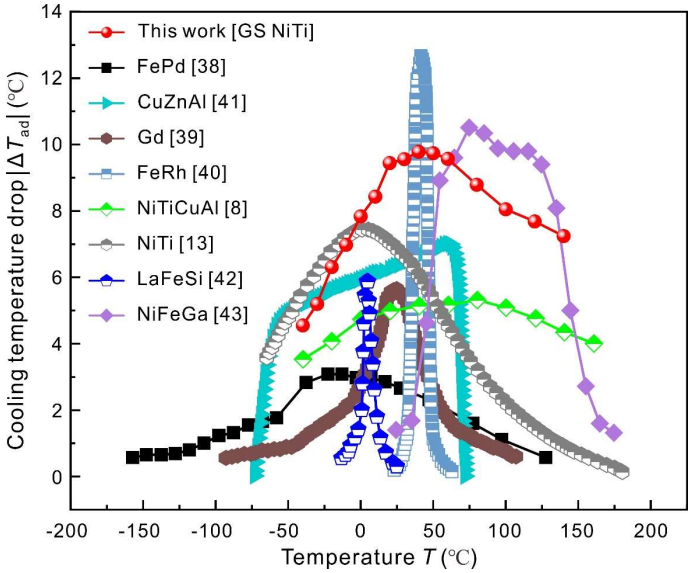

Fig. 5. A comparison of the cooling temperature drop $|\Delta T_{ad}|$ as a function of the ambient temperature T for the GS NiTi and other reported solid-state caloric materials [8, 13, 38-43].

In summary, NiTi with a gradient in the grain structure that was developed by cold rolling and laser surface annealing exhibits large cooling capacity ($|\Delta T_{ad}|$) over a wide service temperature span (T_{span}). The GS NiTi consists of a nanocrystalline core sandwiched by two coarse-grained layers with gradually changing grain sizes from ~12 to 110 nm, and thus exhibits a stable and mild martensitic transformation. Consequently, compared to the conventional coarse-grained NiTi with typical first-order phase

transformation characteristics, GS NiTi shows a substantially larger T_{span} and $|\Delta T_{ad}|$, the combination of which results in a multifold increase in the cooling efficiency. We attribute the outstanding elastocaloric properties to the gradient structure effect, where the fine grains diminish the global martensitic autocatalytic nucleation potency and simultaneously increase strength to widen T_{span}, while the coarse grains activate and accommodate deformation to enhance $|\Delta T_{ad}|$. The work demonstrates a potential strategy to reconcile wide T_{span} and large $|\Delta T_{ad}|$ of the NiTi refrigerant for green elastocaloric cooling, which might inspire the discovery of superior cooling properties in a wide range of ferroelastic materials.

Acknowledgments

This work was supported by the National Key Research and Development Program of China (No. 2017YFB0701801). The work at Nanyang Technological University was supported by the Agency for Science, Technology and Research (A*STAR) of Singapore via the Structural Metal Alloys Programme (No. A18B1b0061).

References

[1] J. Chen, L. Lei, G. Fang, Elastocaloric cooling of shape memory alloys: A review, Mater. Today Commun. 28 (2021) 102706.

[2] H. Hou, E. Simsek, D. Stasak, N.A. Hasan, S. Qian, R. Ott, J. Cui, I. Takeuchi, Elastocaloric cooling of additive manufactured shape memory alloys with large latent heat, J. Phys. D: Appl. Phys. 50(40) (2017) 404001.

[3] H. Hou, E. Simsek, T. Ma, N.S. Johnson, S. Qian, C. Cissé, D. Stasak, N. Al Hasan, L. Zhou, Y. Hwang, R. Radermacher, V.I. Levitas, M.J. Kramer, M.A. Zaeem, A.P. Stebner, R.T. Ott, J. Cui, I. Takeuchi, Fatigue-resistant high-performance elastocaloric materials made by additive manufacturing, Science 366(6469) (2019) 1116-1121.

[4] T. Omori, K. Ando, M. Okano, X. Xu, Y. Tanaka, I. Ohnuma, R. Kainuma, K. Ishida, Superelastic effect in polycrystalline Ferrous alloys, Science 333(6038) (2011) 68-71.

[5] A. Ahadi, T. Kawasaki, S. Harjo, W.-S. Ko, Q. Sun, K. Tsuchiya, Reversible elastocaloric effect at ultra-low temperatures in nanocrystalline shape memory alloys, Acta Mater. 165 (2019) 109-117.

[6] J. Chen, L. Lei, G. Fang, Grain-size effects on the temperature-dependent elastocaloric cooling performance of polycrystalline NiTi alloy, J. Alloys Compd. 927 (2022) 166951.

[7] S. Li, D. Cong, X. Sun, Y. Zhang, Z. Chen, Z. Nie, R. Li, F. Li, Y. Ren, Y. Wang, Wide-temperature-range perfect superelasticity and giant elastocaloric effect in a high entropy alloy, Mater. Res. Lett. 7(12) (2019) 482-489.

[8] H. Chen, F. Xiao, Z. Li, X. Jin, L. Mañosa, A. Planes, Elastocaloric effect with a broad temperature window and low energy loss in a nanograin Ti-44Ni-5Cu-1Al (at·%) shape memory alloy, Phys. Rev. Mater. 5(1) (2021) 015201.

[9] H.-C. Lee, J.-J. Shen, Y.-T. Chang, C.-T. Wu, C.-H. Chen, Evolutions of superelasticity and elastocaloric effect of $Ti_{50}Ni_{48}Fe_2$ and aged-hardened Ni-rich $Ti_{49.2}Ni_{49.3}Fe_{1.5}$ shape memory alloys under cyclic compressive deformation, J. Alloys Compd. 893 (2022) 162352.

[10] H. Zhang, J. Liu, Z. Ma, Y. Ren, D. Jiang, L. Cui, K. Yu, Small stress-hysteresis in a nanocrystalline TiNiCuFe alloy for elastocaloric applications over wide temperature window, J. Alloys Compd. 928 (2022) 167195.

[11] P. Dang, L. Zhang, Y. Zhou, Q. Liang, X. Ding, J. Sun, D. Xue, Cryogenic superelasticity and elastocaloric effect in a nanostructured Ti-Ni-Co alloy, Scr. Mater. 236 (2023) 115638.

[12] J. Chen, L. Lei, G. Fang, D. Wang, Achieving great comprehensive elastocaloric cooling performances of superelastic NiTi by grain size engineering, Mater. Today Nano 21 (2023) 100279.

[13] Z. Deng, K. Huang, H. Yin, Q. Sun, Temperature-dependent mechanical properties and elastocaloric effects of multiphase nanocrystalline NiTi alloys, J. Alloys Compd. 938 (2023) 168547.

[14] J. Chen, B. Liu, L. Xing, W. Liu, L. Lei, G. Fang, Toward tunable mechanical behavior and enhanced elastocaloric effect in NiTi alloy by gradient structure, Acta Mater. 226 (2022) 117609.

[15] J. Chen, L. Xing, G. Fang, L. Lei, W. Liu, Improved elastocaloric cooling performance in gradient-structured NiTi alloy processed by localized laser surface annealing, Acta Mater. 208 (2021) 116741.

[16] Q. Zhang, J. Chen, G. Fang, From mechanical behavior and elastocaloric effect to microscopic mechanisms of gradient-structured NiTi alloy: A phase-field study, Int. J. Plast. 171 (2023) 103809.

[17] J. Chen, C. Zhao, S. Zhang, W. Zhang, W. Liu, L. Lei, U. Ramamurty, G. Fang, Imparting high elastocaloric cooling potential to NiTi alloy by two-step enhancements, Mater. Sci. Eng., A 892 (2024) 146073.

[18] H. Lin, P. Hua, Q. Sun, Effects of grain size and partial amorphization on elastocaloric cooling performance of nanostructured NiTi, Scr. Mater. 209 (2022) 114371.

[19] Q. Sun, A. Ahadi, M. Li, M. Chen, Effects of grain size on phase transition behavior of nanocrystalline shape memory alloys, Sci. China: Technol. Sci. 57(4) (2014) 671-679.

[20] B. Xu, C. Yu, G. Kang, Phase field study on the microscopic mechanism of grain size dependent cyclic degradation of super-elasticity and shape memory effect in nano-

polycrystalline NiTi alloys, Int. J. Plast. 145 (2021) 103075.
[21] J. Zhang, T. Chen, W. Li, J. Bednarcik, A.-C. Dippel, High temperature superelasticity realized in equiatomic TiNi conventional shape memory alloy by severe cold rolling, Mater. Des. 193 (2020) 108875.
[22] K. Otsuka, K. Shimizu, Pseudoelasticity and shape memory effects in alloys, Int. Met. Rev. 31(1) (1986) 93-114.
[23] Y. Liu, S.P. Galvin, Criteria for pseudoelasticity in near-equiatomic NiTi shape memory alloys, Acta Mater. 45(11) (1997) 4431-4439.
[24] S.M. Saghaian, H.E. Karaca, H. Tobe, M. Souri, R. Noebe, Y.I. Chumlyakov, Effects of aging on the shape memory behavior of Ni-rich $Ni_{50.3}Ti_{29.7}Hf_{20}$ single crystals, Acta Mater. 87 (2015) 128-141.
[25] J. Chen, H. Yin, Q. Sun, Effects of grain size on fatigue crack growth behaviors of nanocrystalline superelastic NiTi shape memory alloys, Acta Mater. 195 (2020) 141-150.
[26] A. Ahadi, Q. Sun, Stress hysteresis and temperature dependence of phase transition stress in nanostructured NiTi—Effects of grain size, Appl. Phys. Lett. 103(2) (2013) 021902.
[27] T. Waitz, V. Kazykhanov, H.P. Karnthaler, Martensitic phase transformations in nanocrystalline NiTi studied by TEM, Acta Mater. 52(1) (2004) 137-147.
[28] T. Waitz, T. Antretter, F.D. Fischer, N.K. Simha, H.P. Karnthaler, Size effects on the martensitic phase transformation of NiTi nanograins, J. Mech. Phys. Solids 55(2) (2007) 419-444.
[29] A. Ahadi, Q. Sun, Grain size dependence of fracture toughness and crack-growth resistance of superelastic NiTi, Scr. Mater. 113 (2016) 171-175.
[30] P. Hua, M. Xia, Y. Onuki, Q. Sun, Nanocomposite NiTi shape memory alloy with high strength and fatigue resistance, Nat. Nanotechnol. 16(4) (2021) 409-413.
[31] S. Gollerthan, M.L. Young, K. Neuking, U. Ramamurty, G. Eggeler, Direct physical evidence for the back-transformation of stress-induced martensite in the vicinity of cracks in pseudoelastic NiTi shape memory alloys, Acta Mater. 57(19) (2009) 5892-5897.
[32] M. Fx Wagner, N. Nayan, U. Ramamurty, Healing of fatigue damage in NiTi shape memory alloys, J. Phys. D: Appl. Phys. 41(18) (2008) 185408.
[33] N. Nayan, D. Roy, V. Buravalla, U. Ramamurty, Unnotched fatigue behavior of an austenitic Ni–Ti shape memory alloy, Mater. Sci. Eng., A 497(1) (2008) 333-340.
[34] H. Chen, F. Xiao, X. Liang, Z. Li, Z. Li, X. Jin, T. Fukuda, Giant elastocaloric effect with wide temperature window in an Al-doped nanocrystalline Ti–Ni–Cu shape memory alloy, Acta Mater. 177 (2019) 169-177.
[35] X. Ren, N. Miura, J. Zhang, K. Otsuka, K. Tanaka, M. Koiwa, T. Suzuki, Y.I. Chumlyakov, M. Asai, A comparative study of elastic constants of Ti–Ni-based alloys prior to martensitic transformation, Mater. Sci. Eng., A 312(1) (2001) 196-206.
[36] E.A. Prokofiev, J.A. Burow, E.J. Payton, R. Zarnetta, J. Frenzel, D.V. Gunderov, R.Z. Valiev, G. Eggeler, Suppression of Ni_4Ti_3 precipitation by grain size refinement in Ni-Rich NiTi shape memory alloys, Adv. Eng. Mater. 12(8) (2010) 747-753.
[37] J. Khalil-Allafi, A. Dlouhy, G. Eggeler, Ni_4Ti_3-precipitation during aging of NiTi shape memory alloys and its influence on martensitic phase transformations, Acta Mater. 50(17) (2002) 4255-4274.
[38] F. Xiao, T. Fukuda, T. Kakeshita, X. Jin, Elastocaloric effect by a weak first-order

transformation associated with lattice softening in an Fe-31.2Pd (at.%) alloy, Acta Mater. 87 (2015) 8-14.

[39] S.Y. Dan'Kov, A. Tishin, V. Pecharsky, K. Gschneidner, Magnetic phase transitions and the magnetothermal properties of gadolinium, Phys. Rev. B 57(6) (1998) 3478.

[40] M.P. Annaorazov, K.A. Asatryan, G. Myalikgulyev, S.A. Nikitin, A.M. Tishin, A.L. Tyurin, Alloys of the FeRh system as a new class of working material for magnetic refrigerators, Cryogenics 32(10) (1992) 867-872.

[41] L. Mañosa, S. Jarque-Farnos, E. Vives, A. Planes, Large temperature span and giant refrigerant capacity in elastocaloric Cu-Zn-Al shape memory alloys, Appl. Phys. Lett. 103(21) (2013) 211904.

[42] A. Fujita, S. Fujieda, Y. Hasegawa, K. Fukamichi, Itinerant-electron metamagnetic transition and large magnetocaloric effects in $La(Fe_xSi_{1-x})_{13}$ compounds and their hydrides, Phys. Rev. B 67(10) (2003) 104416.

[43] F. Xiao, M. Jin, J. Liu, X. Jin, Elastocaloric effect in $Ni_{50}Fe_{19}Ga_{27}Co_4$ single crystals, Acta Mater. 96 (2015) 292-300.